

Optimization of whispering gallery resonator design for biosensing applications

T. Reynolds,^{1,*} M. R. Henderson,¹ A. François,¹ N. Riesen,¹ J. M. M. Hall,¹ S. V. Afshar,^{1,3} S. J. Nicholls,² and T. M. Monro^{1,3}

¹The Institute for Photonics and Advanced Sensing (IPAS), and ARC Centre of Excellence for Nanoscale BioPhotonics (CNBP), University of Adelaide, Adelaide SA 5005, Australia

²South Australian Health & Medical Research Institute (SAHMRI), Adelaide SA 5000, Australia

³University of South Australia, Adelaide SA 5000, Australia

* tess.reynolds@adelaide.edu.au

Abstract: Whispering gallery modes (WGMs) within microsphere cavities enable highly sensitive label-free detection of changes in the surrounding refractive index. This detection modality is of particular interest for biosensing applications. However, the majority of biosensing work utilizing WGMs to date has been conducted with resonators made from either silica or polystyrene, while other materials remain largely uninvestigated. By considering characteristics such as the quality factor and sensitivity of the resonator, the optimal WGM sensor design can be identified for various applications. This work explores the choice of resonator refractive index and size to provide design guidelines for undertaking refractive index biosensing using WGMs.

©2015 Optical Society of America

OCIS codes: (070.5753) Resonators; (140.3945) Microcavities; (230.0230) Optical devices; (280.1415) Biological sensing and sensors.

References and links

1. F. Vollmer and S. Arnold, "Whispering-gallery-mode biosensing: label-free detection down to single molecules," *Nat. Methods* **5**(7), 591–596 (2008).
2. P. Zijlstra, K. L. van der Molen, and A. P. Mosk, "Spatial refractive index sensor using whispering gallery modes in an optically trapped microsphere," *Appl. Phys. Lett.* **90**(16), 161101 (2007).
3. A. François, T. Reynolds, and T. M. Monro, "A fiber-tip label-free biological sensing platform: a practical approach toward *in-vivo* sensing," *Sensors (Basel)* **15**(1), 1168–1181 (2015).
4. S. Pang, R. E. Beckham, and K. E. Meissner, "Quantum dot-embedded microspheres for remote refractive index sensing," *Appl. Phys. Lett.* **92**(22), 221108 (2008).
5. S. Arnold, M. Khoshima, I. Teraoka, S. Holler, and F. Vollmer, "Shift of whispering-gallery modes in microspheres by protein adsorption," *Opt. Lett.* **28**(4), 272–274 (2003).
6. M. D. Baaske, M. R. Foreman, and F. Vollmer, "Single-molecule nucleic acid interactions monitored on a label-free microcavity biosensor platform," *Nat. Nanotechnol.* **9**(11), 933–939 (2014).
7. M. I. Cheema, S. Mehrabani, A. A. Hayat, Y. A. Peter, A. M. Armani, and A. G. Kirk, "Simultaneous measurement of quality factor and wavelength shift by phase shift microcavity ring down spectroscopy," *Opt. Express* **20**(8), 9090–9098 (2012).
8. D. W. Vernooy, V. S. Ilchenko, H. Mabuchi, E. W. Streed, and H. J. Kimble, "High-Q measurements of fused-silica microspheres in the near infrared," *Opt. Lett.* **23**(4), 247–249 (1998).
9. J. R. Schwesyg, T. Beckmann, A. S. Zimmermann, K. Buse, and D. Haertle, "Fabrication and characterization of whispering-gallery-mode resonators made of polymers," *Opt. Express* **17**(4), 2573–2578 (2009).
10. F. Vollmer and L. Yang, "Label-free detection with high-Q microcavities: a review of biosensing mechanisms for integrated devices," *Nanophotonics* **1**(3–4), 267–291 (2012).
11. Y. Ruan, K. Boyd, H. Ji, A. François, H. Ebendorff-Heidepriem, J. Munch, and T. M. Monro, "Tellurite microspheres for nanoparticle sensing and novel light sources," *Opt. Express* **22**(10), 11995–12006 (2014).
12. R. S. Moirangthem and A. Erbe, "Interfacial refractive index sensing using visible-excited intrinsic zinc oxide photoluminescence coupled to whispering gallery modes," *Appl. Phys. Lett.* **103**(5), 051108 (2013).
13. A. Paunoiu, R. S. Moirangthem, and A. Erbe, "Whispering gallery modes in intrinsic TiO₂ microspheres coupling to the defect-related photoluminescence after visible excitation," *Phys. Status Solidi RRL* **9**(4), 241–244 (2015).
14. N. M. Hanumegowda, C. J. Stica, B. C. Patel, I. White, and X. D. Fan, "Refractometric sensors based on microsphere resonators," *Appl. Phys. Lett.* **87**(20), 201107 (2005).

15. A. Ksendzov and Y. Lin, "Integrated optics ring-resonator sensors for protein detection," *Opt. Lett.* **30**(24), 3344–3346 (2005).
16. M. L. Gorodetsky and V. S. Ilchenko, "Optical microsphere resonators: optimal coupling to high-Q whispering gallery modes," *J. Opt. Soc. Am. B* **16**(1), 147–154 (1999).
17. Z. Ballard, M. D. Baaske, and F. Vollmer, "Stand-off biodetection with free-space coupled asymmetric microsphere cavities," *Sensors (Basel)* **15**(4), 8968–8980 (2015).
18. M. R. Foreman, W. L. Jin, and F. Vollmer, "Optimizing detection limits in whispering gallery mode biosensing," *Opt. Express* **22**(5), 5491–5511 (2014).
19. M. L. Gorodetsky, A. D. Pryamikov, and V. S. Ilchenko, "Rayleigh scattering in high-Q microspheres," *J. Opt. Soc. Am. B* **17**(6), 1051–1057 (2000).
20. M. L. Gorodetsky, A. A. Savchenkov, and V. S. Ilchenko, "Ultimate Q of optical microsphere resonators," *Opt. Lett.* **21**(7), 453–455 (1996).
21. Z. Guo, H. Quan, and S. Pau, "Near-field gap effects on small microcavity whispering gallery mode resonators," *J. Phys. D Appl. Phys.* **39**(24), 5133–5136 (2006).
22. M. Himmelhaus and A. François, "In-vitro sensing of biomechanical forces in live cells by a whispering gallery mode biosensor," *Biosens. Bioelectron.* **25**(2), 418–427 (2009).
23. I. M. White and X. Fan, "On the performance quantification of resonant refractive index sensors," *Opt. Express* **16**(2), 1020–1028 (2008).
24. J. Hu, X. Sun, A. Agarwal, and L. C. Kimerling, "Design guidelines for optical resonator biochemical sensors," *J. Opt. Soc. Am. B* **26**(5), 1032–1041 (2009).
25. M. I. Cheema, C. Shi, A. M. Armani, and A. G. Kirk, "Optimizing the signal to noise ratio of microcavity sensors," *IEEE Photon. Technol. Lett.* **26**(20), 2023–2026 (2014).
26. H. Chew, "Transition rates of atoms near spherical surfaces," *J. Chem. Phys.* **87**(2), 1355–1360 (1987).
27. H. Chew, "Radiation and lifetimes of atoms inside dielectric particles," *Phys. Rev. A* **38**(7), 3410–3416 (1988).
28. C. F. Bohren and D. R. Huffman, *Absorption and Scattering by a Sphere* (Wiley-VCH Verlag GmbH, 2007).
29. R. Lessard, O. Rousseau-Cyr, M. Charlebois, C. Riviere, O. Mermut, and C. N. Allen, "Flow cytometer system for single-shot biosensing based on whispering gallery modes in fluorescent microspheres," *Proc. SPIE* **8600**, 86001 (2013).
30. J. M. M. Hall, V. Shahraam Afshar, M. R. Henderson, A. François, T. Reynolds, N. Riesen, and T. M. Monro, "Method for predicting whispering gallery mode spectra of spherical microresonators," *Opt. Express* **23**(8), 9924–9937 (2015).
31. V. S. Ilchenko, A. M. Bennett, P. Santini, A. A. Savchenkov, A. B. Matsko, and L. Maleki, "Whispering gallery mode diamond resonator," *Opt. Lett.* **38**(21), 4320–4323 (2013).
32. A. François, N. Riesen, H. Ji, S. Afshar V, and T. M. Monro, "Polymer based whispering gallery mode laser for biosensing applications," *Appl. Phys. Lett.* **106**(3), 031104 (2015).
33. M. Himmelhaus, S. Krishnamoorthy, and A. François, "Optical sensors based on whispering gallery modes in fluorescent microbeads: response to specific interactions," *Sensors (Basel)* **10**(6), 6257–6274 (2010).
34. J. Lutti, W. Langbein, and P. Borri, "High Q optical resonances of polystyrene microspheres in water controlled by optical tweezers," *Appl. Phys. Lett.* **91**(14), 141116 (2007).
35. J. Zhang, L. Xue, and Y. Han, "Fabrication gradient surfaces by changing polystyrene microsphere topography," *Langmuir* **21**(1), 5–8 (2005).
36. G. E. Yakubov, O. I. Vinogradova, and H. J. Butt, "A study of the linear tension effect on the polystyrene microsphere wettability with water," *Colloid J.* **63**(4), 518–525 (2001).
37. L. Xiang, C. Zhuang-Qi, S. Qi-Shun, and Y. Yan-Fang, "Study on the thermo-optic properties of DR1/PMMA composite," *Chin. Phys.* **15**(10), 2439–2444 (2006).
38. S. N. Kasarova, N. G. Sultanova, and I. D. Nikolov, "Temperature dependence of refractive characteristics of optical plastics," *J. Phys. Conf. Ser.* **253**, 012028 (2010).
39. R. Bischler, M. Olszyna, M. Himmelhaus, and L. Dähne, "Development of a fully automated in-vivo diagnostic system based on low-Q whispering gallery modes in fluorescent microparticles," *Eur. Phys. J. Spec. Top.* **223**(10), 2041–2055 (2014).
40. J. R. Schwesyg, T. Beckmann, A. S. Zimmermann, K. Buse, and D. Haertle, "Fabrication and characterization of whispering-gallery-mode resonators made of polymers," *Opt. Express* **17**(4), 2573–2578 (2009).
41. M. Humar, M. Ravnik, S. Pajk, and I. Mušević, "Electronically tunable liquid crystal optical microresonators," *Nat. Photonics* **3**(10), 595–600 (2009).
42. K. Sasagawa, Z.-Yonezawa, R. Iwai, J. Ohta, and M. Nunoshita, "S-band Tm 3+-doped tellurite glass microsphere laser via a cascade process," *Appl. Phys. Lett.* **85**(19), 4325 (2004).
43. A. François, K. J. Rowland, S. V. Afshar, M. R. Henderson, and T. M. Monro, "Enhancing the radiation efficiency of dye doped whispering gallery mode microresonators," *Opt. Express* **21**(19), 22566–22577 (2013).

1. Introduction

The use of whispering gallery modes (WGMs) within microsphere resonators for detecting changes in the surrounding refractive index has been extensively studied and exploited for use in biological sensing [1–6]. The phenomenon of WGMs in microspheres arises from light

being trapped inside the resonator circumference due to total internal reflection. The circulating light has an evanescent field that extends beyond the resonator into the surrounding medium, enabling changes in the surrounding refractive index to be monitored via the shifts in the resonance wavelengths. The addition of surface functionalization to the microsphere allows interaction with specific analytes as they bind to the surface, enabling highly sensitive and selective, label-free detection of molecules to be made [5, 6] down to the single molecule level [6]. The amount of time the light remains circulating within the resonator determines the quality (Q) factor. The Q-factor can be expressed equivalently in terms of a variety of quantities including the cavity ring down time [7], the ratio between resonance wavelength and linewidth, the energy stored in the resonator as well as the loss mechanisms of the resonator (i.e. surface scattering, material absorption and radiation losses) [8]. As the Q-factor increases, the resonance linewidth decreases, enabling smaller wavelength shifts to be measured [5]. Such improvements in the resolution are of particular importance for biosensing applications.

The majority of biosensing work previously conducted utilizing WGMs in microspheres has involved the use of silica [1, 5, 6] or polystyrene [3, 4, 9], with other materials remaining largely uninvestigated [10], apart from a few examples of high refractive index glass [11], ZnO [12] or TiO₂ [13] microspheres. Silica microspheres are usually produced via melting of the tip of an optical fiber [5, 6] and typically range from 50 to 100 μm in diameter [14]. As the microsphere remains attached to the fiber during this fabrication process, it can be secured in position, allowing light from a tunable laser to be coupled evanescently to the microsphere using a phase matched fiber taper [14], waveguide [15] or prism [16]. Free space coupling to microspheres has also recently been demonstrated for the case of asymmetric resonators [17]. Optimization of the sensing performance of silica microspheres has previously been conducted by examining the detection limits [18], as well as increasing the Q-factor by reducing the material absorption and scattering contributions [19]. Q-factors as high as 8×10^9 have been demonstrated using evanescent coupling, closing in on the ultimate Q-factor, as dictated by material attenuation, of 9×10^9 at 633 nm [20].

Despite the extremely high Q-factors that have been recorded using evanescent coupling, the alignment requirements in such systems, impose practical limitations on the use of the sensors. For example, any change in the position of a fiber taper with respect to a microresonator will induce changes in the positions of the resonance peaks due to a change in effective refractive index [21], which may be indistinguishable from changes in refractive index of the surrounding medium or binding events. Furthermore, the fiber taper used for coupling light into the resonator may become contaminated during the sensing experiment, resulting in reduced throughput [17]. In contrast, fluorescence based sensing, such as that involving dye-doped microspheres, alleviates some of the practical constraints by enabling remote interrogation of the WGM modulated fluorescence of the microsphere. However, the significantly lower Q-factors reported for such systems restrict the achievable sensing performance. The finite resolution of the detection system, often a spectrometer for fluorescence-based methods, may also limit the performance.

In order to capitalize on the practical benefits shown by small fluorescent microspheres such as remote excitation and detection [3], which can be used for e.g. interrogating complex phenomenon within living cells [22], different resonator materials and sizes need to be investigated to help bridge the performance gaps between passive (fiber taper or prism coupled) and active (free space coupled fluorescent) microspheres. This could for instance allow for the detection of smaller biomolecules and within lower concentrations even when using active microspheres, matching the performance achieved with fiber taper coupled passive microspheres [1, 6, 7]. The problem of determining the optimal WGM sensor design has been approached previously by considering a variety of different parameters. These include, but are not limited to, the detection limit [23], introducing a new parameter of time normalized sensitivity to allow comparison of sensors in the white-noise-limited regime [24],

and optimizing the signal to noise ratio [25]. Our method of investigating a large range of different resonator refractive indices and sizes is to utilize an analytical model [26, 27], simulating the WGM spectrum as a way towards characterizing the sensing performance by extracting parameters such as the resonator's sensitivity and Q-factor directly from WGM spectra. The model allows for any sphere (refractive index n_l and radius R) to be assessed and compared with any other sphere.

The aim of the current research is to consider a subset of resonators and demonstrate how the model can be applied to provide guidelines for designing WGM based refractive index sensing fluorescent microspheres.

2. Theoretical considerations

The WGM spectrum of a dielectric microsphere of radius R and refractive index n_l can be predicted by extending classical Mie Scattering theory, as illustrated by Chew [26, 27]. Consider an arbitrary distribution of dipoles within a spherical dielectric resonator, of radius R and refractive index n_l , within a medium of refractive index n_2 . The resulting total average power radiated from the sphere is given by the sum of the radial and tangential oscillations, as defined in [27]:

$$P = 2H \sum_{n=1}^{\infty} \frac{2n+1}{3} \left(\frac{J_n}{|D_n|^2} + \frac{GK_n}{|D_n'|^2} \right) \quad (1)$$

where,

$$H = \frac{9\varepsilon_1}{4\rho_1^5} \sqrt{\frac{\varepsilon_1 \varepsilon_2 \mu_1}{\mu_2}}, \quad G = \frac{\mu_1 \mu_2}{\varepsilon_1 \varepsilon_2}$$

$$K_n = \left(\frac{\rho_1^3}{2} \right) \left[j_n^2(\rho_1) - j_{n+1}(\rho_1) j_{n-1}(\rho_1) \right], \quad J_n = K_{n-1} - n\rho_1 j_n^2(\rho_1)$$

$$D_n = \varepsilon_1 j_n(\rho_1) \left[\rho_2 h_n^{(1)}(\rho_2) \right]' - \varepsilon_2 h_n^{(1)}(\rho_2) \left[\rho_1 j_n(\rho_1) \right]', \quad D_n' = D_n(\varepsilon_{1,2} \rightarrow \mu_{1,2})$$

$$\rho_{1,2} = k_{1,2} R$$

where H and G are normalization factors, D_n' and D_n are the electric and magnetic multiple terms (equivalent to the Mie Scattering coefficients), j_n is the n^{th} order spherical Bessel function of the first kind, $h_n^{(1)}$ is the n^{th} order spherical Hankel function of the first kind, $\varepsilon_{1,2}$ and $\mu_{1,2}$ are the permittivity and permeability of the sphere and surrounding medium, respectively, and $\rho_{1,2}$ is the size parameter [27].

The Chew formulation for modeling WGM spectra has previously been shown to be consistent with classical Mie scattering with agreement of the resonance positions [28]. It has also previously been implemented in flow cytometer systems for the efficient identification of the (R, n_l) values of microsphere populations [29]. Recently, we have confirmed that this formulation agrees with other analytical models and also that it is consistent with computational simulations based on the Finite-Difference Time-Domain (FDTD) method [30]. We note here that the FDTD method provides the opportunity to investigate other resonator geometries, as well as provide insight extending beyond the spectral information, including transient phenomena. In contrast, the Chew model is significantly less computationally expensive to run, and hence allows for more efficient scanning over large parameter spaces.

By generating the WGM spectrum of a resonator of any combination of radius and material, it is possible to characterize sensing performance through the calculation of key parameters such as the Q-factor (or components thereof) and refractive index sensitivity. The

overall cavity Q-factor is intrinsically tied to the losses of the resonator and so can be expressed in terms of the individual loss mechanisms involved,

$$\frac{1}{Q} = \frac{1}{Q_m} + \frac{1}{Q_s} + \frac{1}{Q_c} \quad (2)$$

where Q_m is due to material loss, Q_s is due to scattering from surface roughness and Q_c is the geometric (tunneling loss) contribution derived from the Chew model. For a given resonance wavelength λ and linewidth $\Delta\lambda$, Q_c can be calculated directly from the simulated WGM spectrum as,

$$Q_c = \frac{\lambda}{\Delta\lambda} \quad (3)$$

Both λ and $\Delta\lambda$ are determined by Gaussian fitting routines that have been written to analyze the WGM spectra. The Chew model enables calculation of only a single contribution to the total Q-factor, and therefore to create a more realistic model to compare with experimental data, all Q-factor components need to be considered. The limiting factor on Q is often material absorption or surface scattering. The limit of the Q-factor due to material losses can be determined by considering the absorption of light by both the resonator and the surrounding medium using an absorption decay constant α_m , as,

$$Q_m = \frac{2\pi n_1}{\lambda \alpha_m} \quad (4)$$

The absorption decay constant is dependent on how tightly the light is confined within the resonator, the wavelength range, and the environment of the measurement.

Scattering contributions can be calculated by modeling the surface roughness as a changing dielectric constant and it has been used to determine upper limits on the Q-factors of small silica spheres [19]. One expression for the limit of the Q-factor due to surface scattering is,

$$Q_s \approx \frac{3\lambda^3 R}{8n_1 \pi^2 B^2 \sigma^2} \quad (5)$$

where B is the correlation length and σ is the variance of the surface roughness [31].

The refractive index sensitivity is calculated by considering the shift in a resonance wavelength position due to a change in the surrounding refractive index, $S = \Delta\lambda/\Delta n$. By simulating the WGM spectrum, and not just determining the resonance positions, other features such as the change in Q_c can also be tracked, as is demonstrated in Fig. 1(a).

3. Results and discussion

To demonstrate how this model can be used, simulations of microspheres with diameters ranging from $R = 1 - 10 \mu\text{m}$ and refractive indices ranging from $n_1 = 1.45 - 2.0$ residing in water ($n_2 = 1.3325$) were carried out using the analytical model described above, with spectral information over the range of 600-615 nm being generated for every (R, n_1) pair. This parameter set was chosen as the refractive index range allows comparison with previous experimental work based on polystyrene microspheres [3, 4, 22, 32, 33], and the wavelength range selected is a common region for organic dyes such as Nile Red [3, 32] or Coumarin derivatives that have previously been utilized for WGM biosensing [22, 33].

Over the entire parameter space considered, each spectrum produced represents the total average power radiating from the resonator which has been normalized to the power of the dipole sources within the medium [27], indicating that to observe the modulation of the

WGMs on top of the fluorescence background and for it to be above any background noise from the experiment, the peak height must exceed unity. This defines the boundary (black line), as observed in Fig. 2, below which no peaks would be observed experimentally.

For every resonator (R, n_1) within the parameter space, to decrease computation time, an initial WGM spectrum (3750 points) is generated over the wavelength range considered, allowing the approximate positions and intensities of the resonance peaks to be identified. To isolate peaks that would be observable experimentally, a threshold on the spectrum is then introduced, with peaks having a height less than unity not being considered. The selected peaks are then regenerated at a higher resolution to accurately determine their position and linewidth. During the regeneration process, care needs to be taken to ensure only one peak is regenerated at a time. If more than one peak resides within the same wavelength window then the calculation of both Q_c and S will either be incorrect or the single peak fitting formulation will fail. Every eligible peak in the spectrum is considered, with the maximum values of S and Q_c being recorded.

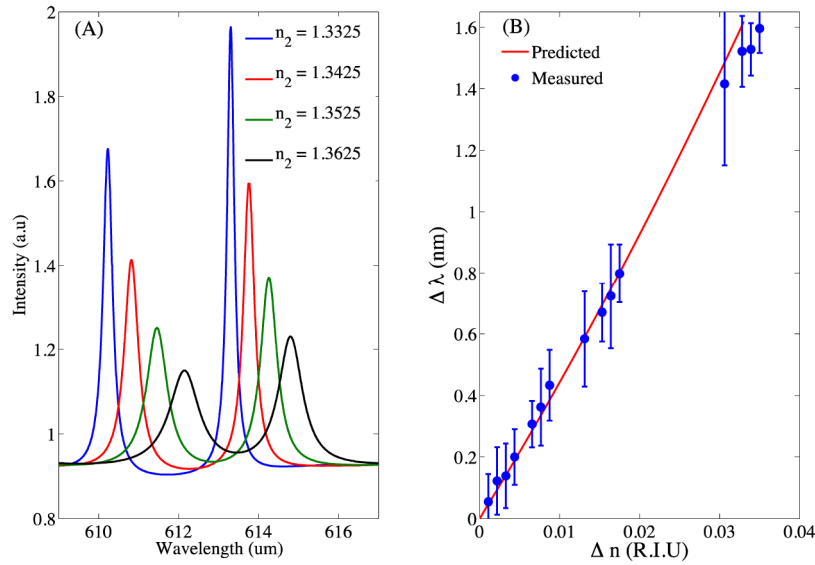


Fig. 1. (a) A demonstration of how the position of the resonance peaks changes for a 5 μm radius polystyrene sphere ($n_1 = 1.59$) initially in water ($n_2 = 1.3325$) for incremental increases in the surrounding refractive index n_2 up to 0.01 R.I.U. (b) Comparison of the predicted sensitivity from the analytical Chew model (red line) with the measured sensitivity for a $R \sim 5$ μm polystyrene sphere in water.

The first feature considered is the refractive index sensitivity. Initially, all the spheres considered reside in water ($n_2 = 1.3325$). In order to calculate S , new spectra are generated after increasing the value of n_2 (step size $\Delta n = 0.0005$ R.I.U.) until the surrounding refractive index has increased by 0.01 R.I.U., monitoring the shift in the position of the resonance peak at each step. An example of this process is shown in Fig. 1(a). The predicted sensitivity for a polystyrene sphere with $R \sim 5$ μm is compared with measured sensitivities, and the result is shown in Fig. 1(b). Excellent agreement is seen between the model and experimental data, therefore validating the numerical model. As expected, the shift in the position of the resonance peaks $\Delta\lambda$ displays a linear response to changes in n_2 over the range of Δn considered, even as Δn extends to values that are higher than those typically observed experimentally for refractive index sensing. The sensitivity of a resonator is related to how tightly the light is confined inside the circumference of the sphere with poor confinement leading to greater sensitivity as more light extends out of the resonator enhancing the interaction with the surrounding environment.

This approach of calculating the sensitivity can be extended to cover the entire parameter space. Figure 2 shows a contour plot of the refractive index sensitivity as functions of radius and refractive index of the resonator. This sensitivity map shows that, for a given sphere radius R , the sensitivity decreases with increasing sphere refractive index, as the increasing index contrast results in the light becoming more tightly confined within the resonator. The region corresponding to the highest sensitivity is located just above the boundary of unit peak height (i.e. black line), and it shows that the higher the refractive index, the smaller the sphere can be whilst maintaining the same sensitivity.

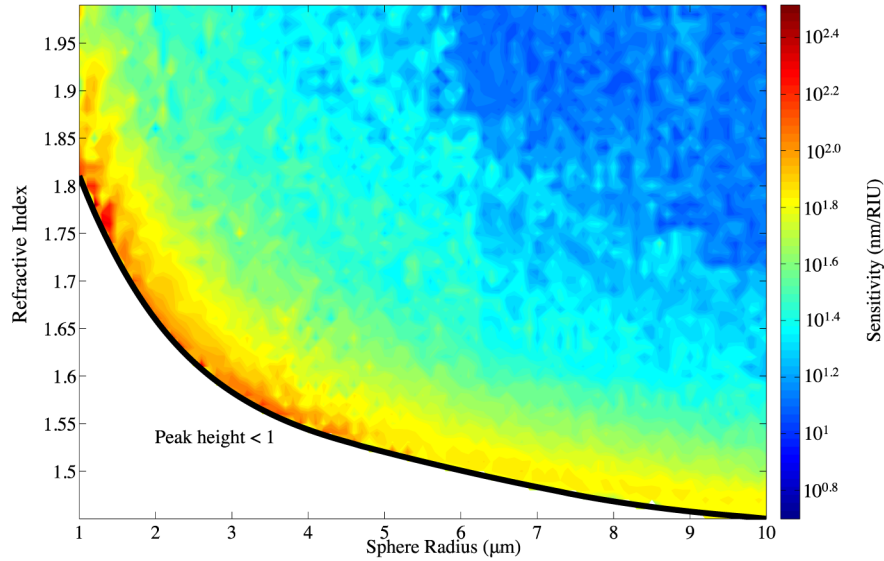


Fig. 2. Contour plot of the sensitivity in nm/RIU., calculated using the analytical Chew model for spherical resonators over the parameter space ranging from $R = 1 - 10 \mu\text{m}$ and microsphere refractive index $n_l = 1.45 - 2.0$ within the wavelength range of 600 – 615 nm.

The Q-factor was also evaluated over the same parameter space as is shown in Fig. 3. Initially, the Q-factor contribution Q_c as derived from the Chew model was determined. Afterwards, other loss mechanisms (e.g. material absorption and surface scattering) can be incorporated as required, but these are strongly dependent on the material properties, nature of the gain medium (organic dye vs quantum dots) and fabrication processes used to produce the microspheres. This implies that Q_c represents an upper limit, for the ideal situation of a perfect sphere with only tunneling losses. In calculating Q_c , every peak within each resonator (R, n_l) spectrum was assessed, and the peak corresponding to the highest Q-factor was recorded as Q_c , noting that this peak is not necessarily the same peak as that of greatest sensitivity. Since we are considering fluorescent microspheres, the maximum Q-factor which can be resolved with the spectrometer (2400 mm^{-1} grating $\sim 4 \text{ pm}$ resolution, 2048 pixels CCD camera) results in the 1.5×10^5 cut-off shown in Fig. 3. Beyond this value of Q-factor, the spectrometer cannot resolve any improvement in WGM linewidth, limiting the benefit of having ultra-high Q resonators in this context.

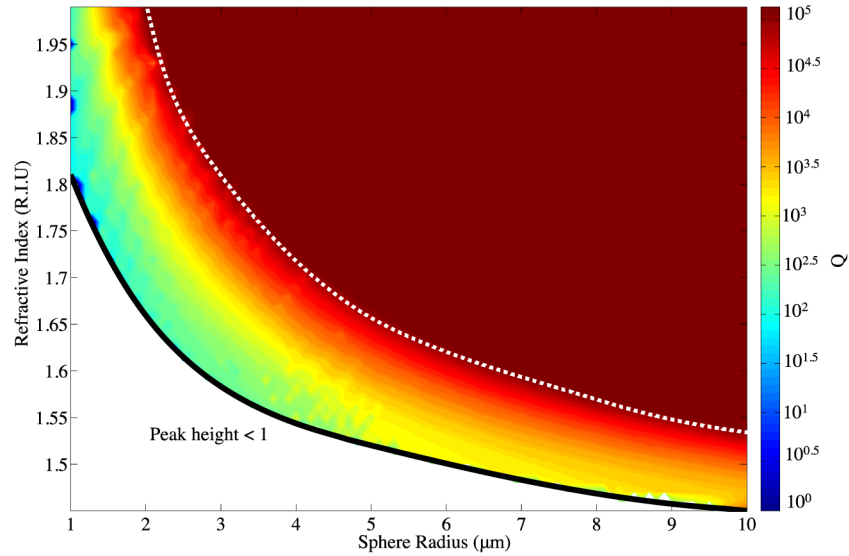


Fig. 3. The quality factor, Q_c , derived using the analytical Chew model for spherical resonators, including the limit placed on the observable Q of fluorescence based microsphere WGMs due to the finite resolution of the spectrometer used (4 pm), over the parameter space ranging from $R = 1 - 10 \mu\text{m}$ and microsphere refractive index range of $n_l = 1.45 - 2.0$, and within the wavelength range of 600-615 nm. The white dotted-line highlights the resolution limit of the spectrometer beyond which any increase in the Q factor cannot be resolved experimentally.

As mentioned, for each specific case the individual loss mechanisms due to surface scattering, material absorption and geometric imperfections can be incorporated providing a more accurate calculation of the total cavity Q -factor. For the present example, focusing on polystyrene microspheres, the loss due to surface scattering was first considered. Q_s was calculated based on the typical surface roughness of polystyrene of 10 nm or greater [34–36]. This results in Q -factor values much larger than that of Q_c (e.g. for $R = 5 \mu\text{m}$, $n_l = 1.59$, $Q_c \sim 4.4 \times 10^3$, $Q_s \sim 5 \times 10^7$) indicating that its contribution to Q through Eq. (2) is insignificant. It is only when the roughness is increased up towards 50 nm, which is unlikely for polystyrene, that Q_s starts to become a limiting factor on the overall Q -factor. For the material losses, it has previously been shown that the intrinsic absorption of polystyrene can be estimated by the typical losses of polymer fibers, corresponding to an absorption coefficient of 0.23 m^{-1} [34], resulting in $Q_m \sim 7.2 \times 10^7$. This is once again orders of magnitude larger, indicating that it too is not the limiting factor on the Q -factor and suggests that another contribution has to be considered.

One possible explanation arises from the fact that the Chew model is based on the assumption that the resonator is perfectly spherical, which in reality is not the case. It is well established that fractional changes in a sphere's radius induces a shift in the resonances. As an example, a $\pm 5 \text{ nm}$ radius deviation for a $R = 5 \mu\text{m}$ polystyrene microsphere results in up to a 0.61 nm wavelength shift. Therefore, we hypothesize that the intrinsic asphericity of a microsphere, falling within the same radius deviation might be the predominant mechanism in lowering the Q -factor of free-floating fluorescent microspheres. For fluorescent microspheres the WGM spectrum originates from all excited equatorial planes. While no discrepancy would be observable for a perfect microsphere, a slightly aspherical one, which can be thought of as having multiple equatorial planes of different effective radius, would exhibit a superposition of perturbed resonances, effectively resulting in the broadening of each individual peak and hence a reduction in the measured Q -factor.

For biological sensing, to achieve the best sensing performance, both high refractive index sensitivity and high Q-factors are required, with the latter dictating the smallest resolvable wavelength shift. However, it appears that the Q-factor and the sensitivity are influenced in very different ways by both the resonator's refractive index and size. Therefore, optimizing the sensing performance requires finding a compromise between these two parameters. Incorporating noise sources, such as, thermal noise, spectral noise and amplitude noise which can be caused either by the optical setup used to interrogate the resonator (e.g. pump power fluctuations, resolution limit of the detector) or by the material constituting the resonator (e.g. thermo optic effect), as shown by White et al. [23], allows for further refinement of the model to be made, but these are specific to individual scenarios. While resonator performance is indeed independent of noise sources specific to individual experimental setups, further consideration of the material properties of the resonator could assist in the sensor design. As an example to highlight this, it is possible to find two materials such as a polymer and a glass (e.g. PMMA and NBK7), which have the same refractive index yet very different thermo optic constants ($-1.20 \times 10^{-4} \text{ K}^{-1}$ [37] and $1.6 \times 10^{-5} \text{ K}^{-1}$ respectively [38]). Nevertheless, as an initial design tool, it is reasonable to compare the sensing performance of the microresonators considered here by using a Figure of Merit (FOM) defined as the product of Q and S, without noise considerations, which fall outside the present scope,

$$FOM = QS \quad (6)$$

On the FOM map shown in Fig. 4, a white dotted-line is shown which corresponds to the maximum FOM ($\sim 6.0 \times 10^6$) achievable for fluorescent microspheres where the maximum resolution of the spectrometer (4 pm with a 2400 mm^{-1} grating and 2400 pixels CCD camera) used to record the WGM spectra will eventually restrict the performance of this sensing approach.

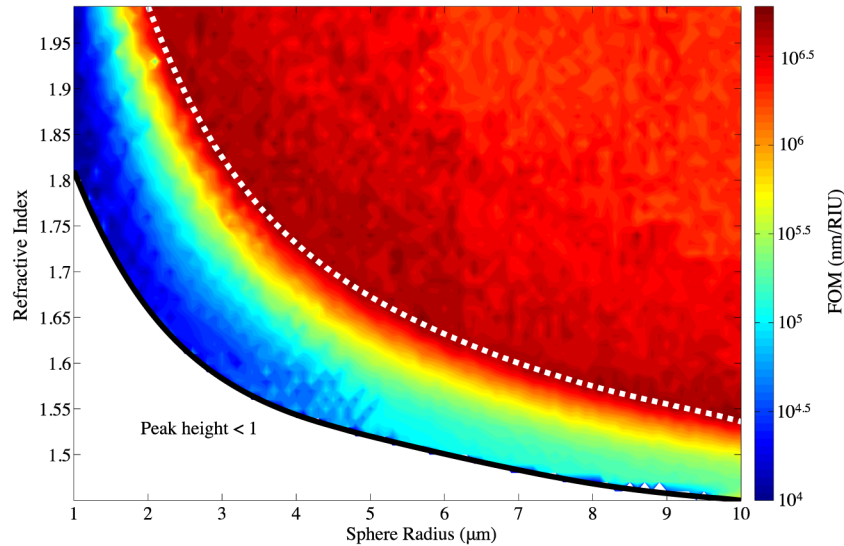


Fig. 4. Figure of Merit (FOM [nm/RI.U.]) mapped over the parameter space $R = 1 - 10 \text{ } \mu\text{m}$ and microsphere refractive index $n_I = 1.45 - 2.0$ within the wavelength range 600-615 nm. The white dotted line represents the maximum value as limited by the spectrometer resolution of 4 pm for fluorescent microspheres.

In order to obtain a high FOM for fluorescent microspheres in water (the typical situation for biosensing applications), spheres with smaller radius and larger refractive indices are required. This could be realized by using materials such as polymers (polystyrene [3, 4, 22, 32, 33], melamine [39], PMMA [40], PDMS [41]), higher refractive index glasses doped with

Erbium [11] or Thulium [42] or other oxides like ZnO [12] or TiOx [13]. The parameter space used in this paper is representative of our previous experiments using dye-doped polystyrene spheres [3, 32], and the results can be used to infer how the performance is likely to compare with other materials. For example, according to the model, a $R = 5\ \mu\text{m}$ melamine ($n_l = 1.68$) sphere will provide a significantly larger FOM (5.05×10^6) compared with a $R = 5\ \mu\text{m}$ polystyrene ($n_l = 1.59$) sphere (2.23×10^5). The FOM map also allows for other resonator material and size combinations to be assessed for specific applications. However the performance is still significantly lower compared to passive microspheres for which the Q-factor is not limited by the resolution of a spectrometer. For instance silica microspheres of $R = 55\ \mu\text{m}$ with a FOM = 1.5×10^8 corresponding to a $Q \sim 5 \times 10^6$ and $S = 30\ \text{nm/R.I.U.}$ have been demonstrated experimentally [14]. This highlights the need for alternative detection modalities for fluorescent microspheres with improved spectral resolution.

While experimentally the Q-factors of fluorescent microspheres are significantly lower than the theoretical values presented here, and as a consequence the FOM is lower than predicted by the model, several improvements are possible. These include operating the active microspheres within their stimulated emission regimes [32] or investigating alternative coupling strategies [43], which result in increased Q-factors.

4. Conclusion

This work represents the first application of the analytical model developed by Chew [26,27] to fluorescence based WGM refractive index biosensors, that allows the sensing performance of any microsphere of refractive index n_l and radius R to be predicted using simulated WGM spectra. The model demonstrates excellent agreement with measured refractive index sensitivity values, whilst providing an upper limit on the achievable resonator Q-factor. By combining the S and Q_c parameters, a Figure of Merit can be given for sensing performance, where additional information specific to the sensing task can be incorporated as required. An example of how this model can be implemented was given, focusing on fluorescence based WGM microspheres. By providing a relatively simple method for generating WGM spectra for any resonator size and material over any given wavelength range, this model serves as an initial step in the resonator selection process for WGM biosensing by predicting the sensitivity and Q-factor for any number of resonators in a range of different situations.

Acknowledgments

The authors acknowledge the support of T.M.M's ARC Georgina Sweet Laureate Fellowship, and the ARC Centre for Nanoscale BioPhotonics. This research was also supported by a grant from the National Breast Cancer Foundation Australia.